JACS
JOURNAL OF THE AMERICAN CHEMICAL SOCIETY

COMMUNICATION

pubs.acs.org/JACS

Fast Formation of SnO_2 Nanoboxes with Enhanced Lithium Storage Capability

Zhiyu Wang,[†] Deyan Luan,[‡] Freddy Yin Chiang Boey,[‡] and Xiong Wen (David) Lou*[,†,§]

[†]School of Chemical and Biomedical Engineering, [‡]School of Materials Science and Engineering, and [§]Energy Research Institute @ NTU, Nanyang Technological University, 70 Nanyang Avenue, Singapore, 637457

Supporting Information

ABSTRACT: SnO_2 nanoboxes with uniform morphology, good structural stability, and tunable interior volume can be facilely synthesized by template-engaged coordinating etching of pregrown Cu_2O nanocubes at room temperature. When evaluated for their lithium storage properties, these SnO_2 nanoboxes manifest improved capacity retention.

Owing to well-defined interior voids, low density, large surface area, and surface permeability, hollow micro/nanostructures have attracted growing research interests in a myriad of applications.[1] A general route toward hollow structures involves the growth of a shell of designed materials on various removable templates including hard templates such as monodispersed silica or polymer latex spheres and soft ones, for example, emulsion micelles and even gas bubbles.[2−8] The use of the templates in principle allows one to manipulate the structure and morphology of resultant hollow particles for greater control of the local chemical environment and extraordinary properties. However, the geometry of hollow products obtained from template-engaged approaches is mostly spherical. Controllable preparation of hollow structures with other shapes still suffer from many difficulties ranging from forming uniform coating around high-curvature surfaces to the paucity of nonspherical templates available.[1] Recently, more novel approaches based on different principles such as galvanic replacement, chemical etching, Kirkendall effect, solid-state decomposition, and self-assembly of nanoparticles have been employed for synthesizing nonspherical nanocages of various materials such as noble metals, transition metal oxides and sulfides.[9−19] No matter the methods adopted, the fundamental driving force for creating hollow cavities is the difference between shell material (or its precursor) and the template in physicochemical stability or reactivity. Here we demonstrate another facile strategy for preparing uniform nanoboxes of metal oxides by combining controlled hydrolysis of corresponding metal ions and simultaneous coordinating etching of the sacrificial template. We choose SnO_2 to demonstrate the concept in view of the limited success in synthesizing nonspherical SnO_2 hollow structures and its expanding technological applications in various fields. As an example, we show that the as-prepared SnO_2 nanoboxes exhibit improved electrochemical properties when evaluated as anode materials in lithium-ion batteries (LIBs).

Coordinating dissolution is commonly used for dissolving many insoluble materials such as cuprous or silver halide, which can coordinate with certain ligands (Cl^-, CN^-, SCN^-, $S_2O_3^{2-}$ or ammonia, etc.) in solution forming soluble complexes.[20,21] Using coordination chemistry, it is possible to create hollow structures through controlled reactions between appropriate ligands and template materials or reaction intermediates. In the case of SnO_2 nanoboxes, the synthetic strategy is designed on the basis of the interplay and synergy of precisely controlled hydrolysis of Sn^{4+} and coordinating etching of Cu_2O nanocubes, as schematically illustrated in Scheme 1. Driven by interfacial reaction between aqueous solution of $SnCl_4$ and solid Cu_2O crystal, SnO_2 precipitation layer is formed around the scaffold of Cu_2O template through accelerated hydrolysis of Sn^{4+} in solution (eq 1). As the intermediate, insoluble CuCl is generated in this process and is simultaneously dissolved in aqueous solution of NaCl by coordinating with Cl^- to form soluble $[CuCl_x]^{1-x}$ (eq 2),[22] consequently, void space emerges within SnO_2 shells as a result of outward flow of $[CuCl_x]^{1-x}$ and inward flow of Sn^{4+} and Cl^-, eventually leading to complete consumption of Cu_2O templates. The overall chemical route for the formation of SnO_2 nanoboxes might be described as follows:

Scheme 1. Schematic Illustration of the Formation of SnO_2 Nanoboxes by Template-Engaged Coordinating Etching of Cu_2O Nanocubes

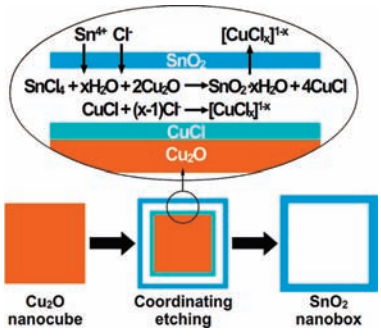

$$SnCl_{4(aq)} + xH_2O + 2Cu_2O_{(s)} \rightarrow SnO_2 \cdot xH_2O_{(s)} + 4CuCl_{(s)} \quad (1)$$

$$CuCl_{(s)} + (x-1)Cl^-_{(aq)} \rightarrow [CuCl_x]^{1-x}_{(s)} \quad (2)$$

During this process, the effect of acidic etching can be ruled out because even all the H^+ ions released from the hydrolysis of Sn^{4+}

Received: January 16, 2011
Published: March 14, 2011

ACS Publications © 2011 American Chemical Society

dx.doi.org/10.1021/ja2004329 | J. Am. Chem. Soc. 2011, 133, 4738–4741

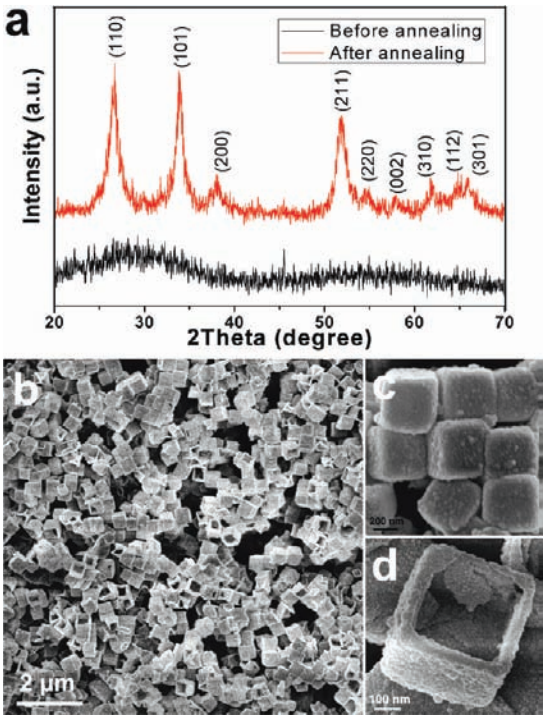

Figure 1. (a) Overview SEM image of the sample; (b) SEM image of several SnO_2 nanoboxes with uniform dimensions; (c) SEM image of a cracked nanobox showing the exposed interior.

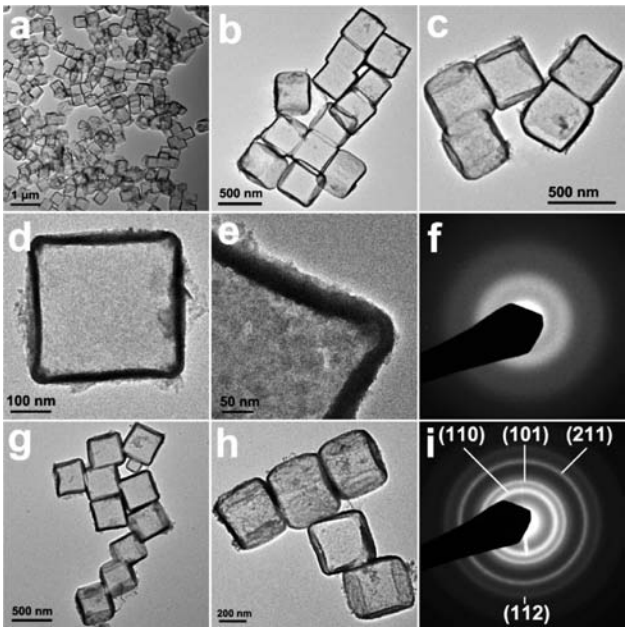

Figure 2. (a) Low-magnification TEM image of as-prepared SnO_2 nanoboxes; (b, c) enlarged TEM images of the nanoboxes at different magnifications; (d) a nanobox with well-defined interior and very thin shell; (e) shell structure of a nanobox; (f) SAED pattern of as-prepared nanoboxes; TEM images (g, h) and SAED pattern (i) of SnO_2 nanoboxes annealed in air at 500 °C.

are quickly consumed by reacting with Cu_2O, at least double amount of $SnCl_4$ (from a simple estimation) is required for complete dissolution of Cu_2O by acidic etching. On the other hand, it should be noted that the reaction is completed rapidly (within 5 min) without addition of any oxidizing agents; oxygen-oxidative or redox etching also appears irrelevant for the emergence of hollow interiors. In this regard, the mechanism involved in the present system is principally different from the known ones based on acidic or oxidative/redox etching of metal oxide templates.[11−13,19]

The crystallographic structure and phase purity of SnO_2 nanoboxes are examined by X-ray powder diffraction (XRD), as shown in Figure 1a. The as-prepared sample is expectedly amorphous in nature because the synthesis is carried out at room temperature. The signals from the Cu_2O phase entirely disappear giving a plain pattern with a broad peak between 20 and 40°. No signals from possible impurities such as CuCl are detected. After controlled annealing at 500 °C in air, the crystallinity of SnO_2 nanoboxes becomes pronounced as evidenced by the increased intensity of the diffraction peaks, especially the (110), (101), and (211) peaks from tetragonal SnO_2 (JCPDS no. 41-1445). During the annealing, a weight loss of around 8−15 wt % is observed by thermogravimetric analysis (TGA) conducted in N_2 due to the removal of crystalline and adsorbed water (Figure S1, Supporting Information [SI]). A panoramic view reveals that the sample consists entirely of uniform nanoboxes without impurity particles or aggregates, as shown in the scanning electron microscopy (SEM) images (Figure 1b,c). The nanoboxes well inherit the uniform dimensions of Cu_2O nanocubes with edge length of around 350 to 400 nm. Their interior space can be examined directly by SEM for cracked nanoboxes, as shown in Figure 1d. The collapse of these nanoboxes may be caused by rapid mass transport across the walls during fast dissolution of the Cu_2O template. The other plausible reason is due to the local aggregation of Cu_2O nanocube templates as observed in the SEM images (Figure S2, SI).

The hollow interior and geometrical structure of as-synthesized SnO_2 nanoboxes are further elucidated by transmission electron microscopy (TEM), as displayed in Figure 2. In agreement with the above SEM findings, a high uniformity of the nanoboxes can be seen from the image, and the inner cavity is clearly revealed by the contrast between SnO_2 shells and hollow interiors. The wall of the nanoboxes is as thin as about 10 to 20 nm due to the short period of precipitation during synthesis. The nanoboxes well duplicate the cubic morphology of Cu_2O templates and the surface is relatively smooth without opening characteristics. No structural degradation such as collapse or amalgamation occurs although the reaction proceeds quite fast. The selected area electron diffraction (SAED) analysis (Figure 2f) indicates the amorphous feature of these nanoboxes, consistent with the above XRD analysis. Despite of being very thin and amorphous, SnO_2 shells possess good structural stability and are found robust enough to withstand thermal annealing at 500 °C (Figure 2g, 2h). After annealing, polycrystalline SnO_2 nanoboxes are obtained without apparent collapse, as evidenced by SAED analysis (Figure 2i) and high-resolution TEM examination (Figure S3, SI). In virtue of the unique hollow structure and small crystallite size, the nanoboxes possess a relatively large Brunauer−Emmett−Teller (BET) surface area of around 60 $m^2 g^{-1}$ (Figure S4, SI). Furthermore, the use of pregrown Cu_2O templates also allows the dimensions and interior volume of resultant nanoboxes to be rationally controlled. For example, SnO_2 nanoboxes with edge lengths of around 200 to 250 and 800 nm to 1 μm can be fabricated using the same route by

dx.doi.org/10.1021/ja2004329 |J. Am. Chem. Soc. 2011, 133, 4738–4741

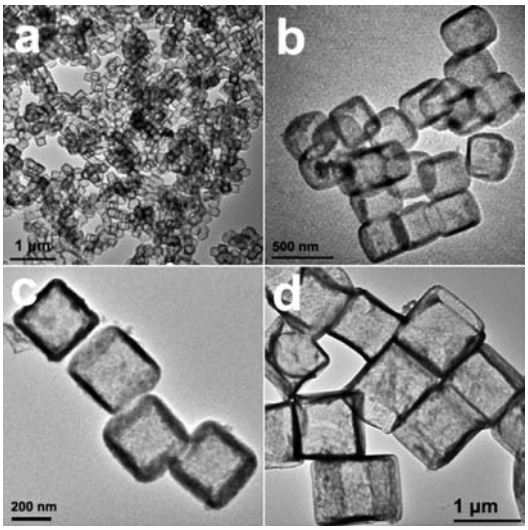

Figure 3. TEM images of SnO_2 nanoboxes with different edge lengths: (a−c) 200−250 nm; (d) 800−1000 nm.

templating against Cu_2O nanocubes with corresponding sizes (Figure 3).

In the present strategy, precise control on the hydrolysis of Sn^{4+} is crucial for producing high-quality SnO_2 nanoboxes. Excessively fast hydrolysis causes inevitable formation of abundant irregular impurities in solution and further induces severe collapse of hollow structures upon rapid mass transport across the shells (Figure S5, SI). Therefore, a proper amount of nonaqueous solvent such as ethanol should be introduced into the reaction system to slow down the hydrolysis of Sn^{4+} so that nanoscale deposition can occur preferentially on the accessible surface of templates to construct conformal shells.[19] In this work, the initial volume ratio of ethanol and water is optimized to be 100:3 to ensure the precipitation of SnO_2 to take place at an appropriate rate. No deposition occurs in pure ethanol because the hydrolysis of Sn^{4+} does not happen.

In an ethanol-rich system with decreased ionizability, the etching of Cu_2O templates is significantly inhibited due to the lack of ionic species in solution. Hence, strong inorganic electrolytes such as NaCl should be introduced to improve the ionic strength of the solution.[19] At the same time, the NaCl in solution also releases sufficient Cl^- to dissolve the insoluble reaction intermediate (CuCl) by forming soluble $[CuCl_x]^-$ complexes (eq 2), which is responsible for the formation of hollow interiors. To verify the dual roles played by NaCl in the formation of SnO_2 nanoboxes, experiments with the same molar concentration of other inorganic electrolytes such as KCl and $NaNO_3$ or without any electrolytes are exploited while other conditions are kept the same. In the presence of KCl in solution, SnO_2 nanoboxes can also be made following the same route despite of the slight difference in product quality (Figure S6a and S6b). When $NaNO_3$ is used, few hollow structures are formed besides partially etched Cu_2O cubes and large quantities of irregular impurities (Figure S6c). Without the introduction of any electrolytes, hollow structures are hardly formed due to the slow etching rate (Figure S6d). In brief, the presence of NaCl in solution not only offers an appropriate ionic environment for the etching of Cu_2O crystals, but also provides an effective coordinating ligand for dissolving the insoluble reaction intermediate. As a result, well-defined SnO_2 nanoboxes are produced under optimized conditions by

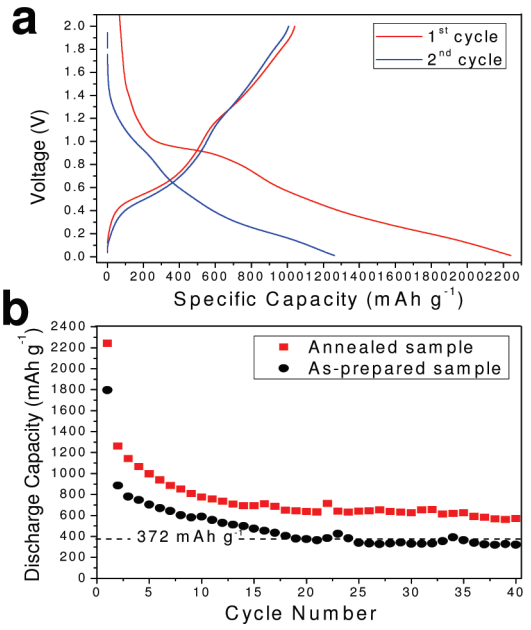

Figure 4. (a) Discharge/charge voltage profiles of annealed SnO_2 nanoboxes cycled between 0.01and 2.0 V at a 0.2 C rate; (b) cycling performance of as-synthesized and annealed SnO_2 nanoboxes at 0.2 C.

utilizing the interplay and synergy of coordinating etching and hydrolysis reaction.

SnO_2 is a very appealing candidate as a substitute of the conventional graphite-based anode in LIBs because of its high theoretical capacity (782 mA h g^{-1}) and improved safety.[23] However, large and uneven volume changes take place upon lithium insertion/extraction within SnO_2, resulting in electrode pulverization and electrical connectivity loss. Macroscopically this is manifested as poor cycling capability. Hollow structures have been exploited to effectively mitigate this problem due to the enhanced kinetics and structural stability for lithium storage.[24−26] The large surface area endows with high capacity and favorable response to high-rate cycling due to dramatic increment of reactive sites and interface between active materials and the electrolyte. The presence of permeable thin walls makes the lithium ion diffusion much easier by shortening the diffusion length effectively to grain size (typically a few nm). The interior space allows the volume variation upon insertion/extraction of lithium ions to be better accommodated. Motivated by the potential of hollow structures for lithium storage, we have evaluated the electrochemical properties of annealed SnO_2 nanoboxes. Figure 4a shows representative discharge/charge voltage profiles of annealed SnO_2 nanoboxes at a 0.2 C rate within a cutoff window of 0.01−2.0 V. The initial discharge and charge capacities are found to be 2242 and 1041 mAh g^{-1}, respectively. Such a high initial lithium storage capacity might be associated with the unique structure of the hollow nanoboxes with nanoporous shells formed during mass transport across them,[23] and has also been observed in many other SnO_2 hollow nanostructures.[24,26−29] The large capacity loss in the first cycle is mainly attributed to the initial irreversible formation of Li_2O, and other irreversible processes such as trapping of some lithium in the lattice, inevitable formation of solid electrolyte interface (SEI layer) and electrolyte decomposition, which are common for most anode materials.[23−26,30,31] From the second cycle onward, the

dx.doi.org/10.1021/ja2004329 |J. Am. Chem. Soc. 2011, 133, 4738–4741

capacity fades gradually to about 570 mA h g^{-1} over 40 cycles (Figure 4b). This value is much higher than the theoretical capacity of graphite (372 mA h g^{-1}). When cycled at a high rate of 0.5 C, comparable capacities of over 510 mA h g^{-1} can still be retained and a capacity of over 470 mAh g^{-1} could be restored at 0.2 C again (Figure S7, SI). For the as-synthesized nanoboxes (without annealing), the capacity decay is much fast but the capacity after 30−40 cycles is still comparable to that of graphite. The may be ascribed to the poor crytallinity and the presence of appreciable amount of water within the as-prepared hydrated tin oxide ($SnO_2 \cdot xH_2O$). Consistent with previous reports, the formation of hollow structures can greatly improve the electrochemical performance of Sn-based anode materials.

In summary, we have demonstrated a facile strategy for fast formation of SnO_2 nanoboxes with uniform morphology, good structural stability and tunable interior volume by template-engaged coordinating etching of pregrown Cu_2O nanocubes at room temperature. Remarkably, the construction of SnO_2 nanoboxes is achieved in a one-step process, which demands careful tuning of many experimental conditions. Specifically, the simultaneous controlled hydrolysis of Sn^{4+} ions and chloride ion-induced coordinating etching of formed insoluble intermediate are crucial for the formation of SnO_2 nanoboxes. When evaluated as potential anode materials for LIBs, the annealed SnO_2 nanoboxes exhibit high lithium storage capacity and excellent cycling performance. A perhaps obvious appeal of our approach is that it can be extended to generate nanoboxes of other metal oxides, such as ZrO_2, as suggested by our preliminary results (Figure S8, SI).

■ ASSOCIATED CONTENT

Supporting Information. Detailed experimental procedures, TGA/BET/TEM/SEM data, as well as electrochemical data. This material is available free of charge via the Internet at http://pubs.acs.org.

■ AUTHOR INFORMATION

Corresponding Author
xwlou@ntu.edu.sg

■ ACKNOWLEDGMENT

We are grateful to the Nanyang Technological University and Ministry of Education (Singapore) for financial support through the start-up grant (SUG) and AcRF Tier-1 funding (RG 63/08, M52120096), respectively.

■ REFERENCES

(1) Lou, X. W.; Archer, L. A.; Yang, Z. C. *Adv. Mater.* **2008**, *20*, 3987.
(2) Kim, S. W.; Kim, M.; Lee, W. Y.; Hyeon, T. *J. Am. Chem. Soc.* **2002**, *124*, 7642.
(3) Caruso, F.; Caruso, R. A.; Mohwald, H. *Science* **1998**, *282*, 1111.
(4) Zoldesi, C. I.; Imhof, A. *Adv. Mater.* **2005**, *17*, 924.
(5) Walsh, D.; Lebeau, B.; Mann, S. *Adv. Mater.* **1999**, *11*, 324.
(6) Peng, Q.; Dong, Y. J.; Li, Y. D. *Angew. Chem., Int. Ed.* **2003**, *42*, 3027.
(7) Zhong, Z. Y.; Yin, Y. D.; Gates, B.; Xia, Y. N. *Adv. Mater.* **2000**, *12*, 206.
(8) Liu, J.; Qiao, S. Z.; Hartono, S. B.; Lu, G. Q. *Angew. Chem., Int. Ed.* **2010**, *49*, 4981.
(9) Skrabalak, S. E.; Chen, J. Y.; Sun, Y. G.; Lu, X. M.; Au, L. S.; Cobley, C. M.; Xia, Y. N. *Acc. Chem. Res.* **2008**, *41*, 1587.
(10) Sun, Y. G.; Mayers, B. T.; Xia, Y. N. *Nano Lett.* **2002**, *2*, 481.
(11) Sui, Y. M.; Fu, W. Y.; Zeng, Y.; Yang, H. B.; Zhang, Y. Y.; Chen, H.; Li, Y. X.; Li, M. H.; Zhou, G. T. *Angew. Chem., Int. Ed.* **2010**, *49*, 4282.
(12) Kuo, C. H.; Huang, M. H. *J. Am. Chem. Soc.* **2008**, *130*, 12815.
(13) An, K.; Kwon, S. G.; Park, M.; Bin Na, H.; Baik, S. I.; Yu, J. H.; Kim, D.; Son, J. S.; Kim, Y. W.; Song, I. C.; Moon, W. K.; Park, H. M.; Hyeon, T. *Nano Lett.* **2008**, *8*, 4252.
(14) Cao, H. L.; Qian, X. F.; Wang, C.; Ma, X. D.; Yin, J.; Zhu, Z. K. *J. Am. Chem. Soc.* **2005**, *127*, 16024.
(15) Wang, L. Z.; Tang, F. Q.; Ozawa, K.; Chen, Z. G.; Mukherj, A.; Zhu, Y. C.; Zou, J.; Cheng, H. M.; Lu, G. Q. *Angew. Chem., Int. Ed.* **2009**, *48*, 7048.
(16) Yang, H. G.; Zeng, H. C. *Angew. Chem., Int. Ed.* **2004**, *43*, 5930.
(17) He, T.; Chen, D. R.; Jiao, X. L.; Wang, Y. L. *Adv. Mater.* **2006**, *18*, 1078.
(18) Jiao, S. H.; Xu, L. F.; Jiang, K.; Xu, D. S. *Adv. Mater.* **2006**, *18*, 1174.
(19) Wang, Z. Y.; Luan, D. Y.; Li, C. M.; Su, F. B.; Madhavi, S.; Boey, F. Y. C.; Lou, X. W. *J. Am. Chem. Soc.* **2010**, *132*, 16271.
(20) Ramanathan, E. *AIEEE Chemistry*; Sura Books: Chennai, 2006: p 245.
(21) Fresenius, C. R. *Quantitative Chemical Analysis*; J. Wiley & sons: New York, 1906; p 236.
(22) Fritz, J. J. *J. Chem. Eng. Data* **1982**, *27*, 188.
(23) Wang, C.; Zhou, Y.; Ge, M. Y.; Xu, X. B.; Zhang, Z. L.; Jiang, J. Z. *J. Am. Chem. Soc.* **2010**, *132*, 46.
(24) Lou, X. W.; Wang, Y.; Yuan, C. L.; Lee, J. Y.; Archer, L. A. *Adv. Mater.* **2006**, *18*, 2325.
(25) Lee, K. T.; Jung, Y. S.; Oh, S. M. *J. Am. Chem. Soc.* **2003**, *125*, 5652.
(26) Ye, J. F.; Zhang, H. J.; Yang, R.; Li, X. G.; Qi, L. M. *Small* **2010**, *6*, 296.
(27) Deng, D.; Lee, J. Y. *Chem. Mater.* **2008**, *20*, 1841.
(28) Lou, X. W.; Deng, D.; Lee, J. Y.; Archer, L. A. *Chem. Mater.* **2008**, *20*, 6562.
(29) Han, S. J.; Jang, B. C.; Kim, T.; Oh, S. M.; Hyeon, T. *Adv. Funct. Mater.* **2005**, *15*, 1845.
(30) Shi, Y. F.; Guo, B. K.; Corr, S. A.; Shi, Q. H.; Hu, Y. S.; Heier, K. R.; Chen, L. Q.; Seshadri, R.; Stucky, G. D. *Nano Lett.* **2009**, *9*, 4215.
(31) Park, M. S.; Wang, G. X.; Kang, Y. M.; Wexler, D.; Dou, S. X.; Liu, H. K. *Angew. Chem., Int. Ed.* **2007**, *46*, 750.